



1 Permafrost degradation of peatlands in northern Sweden

2 **Authors:** Samuel Valman^{1,2*}, Matthias Siewert^{3*}, Doreen Boyd², Martha Ledger^{4,5}, David
3 Gee⁶, Betsabe de la Barreda-Bautista^{4,2}, Andrew Sowter⁶, Sofie Sjogersten⁴

4 **Affiliations:**

5 ¹ Nottingham Geospatial Institute, University of Nottingham, Nottingham NG7 2TU, UK

6 ² School of Geography, University of Nottingham, University Park, NG7 2RD, Nottingham, UK

7 ³ Department of Ecology and Environmental Sciences, Umeå University, Umeå, Sweden

8 ⁴ School of Biosciences, University of Nottingham, Sutton Bonington Campus, College Road, LE12 5RD,
9 Loughborough, UK

10 ⁵ School of Biological Sciences, Kadoorie Biological Sciences Building, University of Hong Kong, Pok Fu Lam
11 Road, Hong Kong

12 ⁶ TerraMotion, Ingenuity Centre, Triumph Rd, Nottingham NG7 2TU

13

14 *These authors contributed equally to this work.

15 Corresponding author: Sofie Sjogersten sofie.sjogersten@nottingham.ac.uk

16 **Abstract.** Climate warming is degrading palsa peatlands across the circumpolar permafrost region. Permafrost
17 degradation may lead to ecosystem collapse and potentially strong climate feedbacks, as this ecosystem is an
18 important carbon store and can transition to being a strong methane emitter. Landscape level measurement of
19 permafrost degradation is needed to monitor this impact of warming. Surface subsidence is a useful metric of
20 change and can be monitored using InSAR satellite technology. We combined InSAR data, processed using the
21 ASPIS algorithm to monitor ground motion between 2017 and 2021, with optical and LiDAR data to investigate
22 the rate of subsidence across palsa peatlands in northern Sweden. We show that 55% of the area of Sweden's
23 eight largest palsa peatlands is currently subsiding, which can be attributed to these permafrost landforms and
24 their degradation. The most rapid degradation occurring in the largest palsa complexes in the most northern part
25 of the region of study, also corresponding to the areas with the highest % palsa cover within the overall mapped
26 wetland area. Further, higher degradation rates were found in areas where winter precipitation has increased
27 substantially. The roughness index calculated from a LiDAR-derived DEM, used as a proxy for degradation,
28 increases alongside subsidence rates and may be used as a complementary proxy for palsa degradation. We
29 show that combining datasets captured using remote sensing enables regional-scale estimation of ongoing
30 permafrost degradation, an important step to-wards estimating the future impact of climate change on
31 permafrost-dependent ecosystems.

32

33 **Keywords:** Permafrost, subsidence, Arctic, InSAR, palsa, peatlands

34



35

36 1.0 Introduction

37 Permafrost regions are critical components in the climate system, due to their essential carbon (C) storage
38 service (Harris et al., 2022). The circumpolar permafrost region in particular, stores around 1300 ± 200 Pg of
39 organic C, corresponding to around 50% of the global terrestrial C pool (Hugelius et al., 2020; Köchy et al.,
40 2015). It covers around 21 million km² or 22% of the Northern Hemisphere's landscapes (Obu, 2021). Northern
41 peatlands themselves store an estimated 415 ± 150 Pg of C in an area covering around 3.7 million km² of which
42 around 1.7 million km² is permafrost substantially overlapping with the circumpolar permafrost region
43 (Hugelius et al., 2020). Permafrost in these peatlands raises the surface above the water table forming so-called
44 *palsa* (pl. *palsas*) or, in extended form peat plateaus (Seppälä, 2011). These account for substantial areas of
45 global permafrost, including in northern Fennoscandia (Ballantyne C. K., 2018; Gislén et al., 2017; Tarnocai et
46 al., 2009), for example, in northern Sweden 137 km² of this *palsa* peatland has been reported (Backe, 2014).
47 Climate warming, and the associated alteration in the precipitation regime, is increasingly recognized to be a
48 particular threat to permafrost (Biskaborn et al., 2019), with the subarctic Fennoscandian permafrost region, and
49 the *palsa* peatlands within, particularly vulnerable (Christiansen et al., 2010; Farbrøt et al., 2013).

50 Climatic models project unsuitable conditions for permafrost within the coming century, with the most pessimistic
51 estimates projecting unsuitability even sooner - by 2040 (Chadburn et al., 2017; Fewster et al., 2022; Könönen et
52 al., 2022; Stefan et al., 2006). As *palsa* peatlands are often found in the sporadic or discontinuous permafrost zone
53 (Zuidhoff & Kolstrup, 2000), they are particularly sensitive to climate warming and any resultant permafrost thaw
54 and disappearance. Their sensitivity mainly results from the alterations in the thermal insulation effect of peat
55 deposits and snow as the climate changes (Seppälä, 2011; Smith & Riseborough, 1996). Specifically, organic peat
56 has a high thermal conductivity when wet and frozen, but low conductivity when dry and thawed. Snow has a
57 highly insulating effect on ground temperature. Thus, extended periods of air-temperatures below 0°C and thin
58 snow cover in winter are beneficial to maintain or grow the frozen permafrost core of *palsas* and peat plateaus.
59 Low summer precipitation, which reduces the thermal conductivity of peat, also helps to preserve the frozen cores
60 in *palsa*. In contrast, increased snowfall has been linked to permafrost degradation as it increases winter insulation.
61 Further, high summer precipitation leads to higher thermal conductivity of peat, and combined with warm summer
62 temperatures, can degrade permafrost by increasing permafrost temperatures and subsequent thawing of the frozen
63 peat core of *palsas*. The strong insulating properties of peat allow the occurrence of permafrost at the southern
64 extent of the northern permafrost region and valley bottoms in areas otherwise too warm for permafrost (Johansson
65 et al., 2013; Seppälä, 2011; Smith & Riseborough, 1996).

66 Warming of the permafrost in *palsa* peatlands typically leads to top-down thaw, (i.e. thickening of the active
67 layer), and eventual subsidence of the surface, as well as lateral thaw, sometimes called abrupt thaw or
68 thermokarst, which occurs at the margin of peat plateaux (Seppälä, 2011; Smith & Riseborough, 1996; Zuidhoff,
69 2002). This is often associated with water-logged conditions and, as a result, increased methane (CH₄) emissions
70 (Glagolev et al., 2011; Hugelius et al., 2020; Matthews et al., 1997; Miglovetz et al., 2021; Schuur et al., 2009;
71 Turetsky et al., 2020; Varner et al., 2022), which is a central theme for permafrost research (Sjöberg *et al.*,
72 2020). A subsequent impact of this permafrost degradation is an alteration in vegetation cover, its hydrology,
73 and human use of the landscape (e.g., infrastructure and reindeer husbandry)(Markkula et al., 2019; Ramage et
74 al., 2021). Given the potentially large impacts of permafrost thaw on the global climate, ecosystem function and
75 human activity, quantification and monitoring of the subsidence in peat deposits affected by permafrost thaw
76 and degradation, as well as an understanding of their sensitivity to changing climatic parameters, is urgently
77 required (IPCC, 2021).

78 The degradation of the permafrost of *palsa* peatlands has been observed right across the circumpolar permafrost
79 region in a number of studies, including in northern Scandinavia (Åkerman & Johansson, 2008; de la Barreda-
80 Bautista et al., 2022; Luoto & Seppälä, 2003; Olvmo et al., 2020; Sannel et al., 2016; Varner et al., 2022);
81 Russia (Glagolev et al., 2011; Miglovetz et al., 2021; van Huissteden et al., 2021); the USA (Douglas et al.,
82 2021; Douglas et al., 2015; Sannel, 2020) and Canada (Mamet et al., 2017; Sannel & Kuhry, 2011; Short et al.,



83 2014; Vallée & Payette, 2007). Although rapid degradation in response to short term climatic events has been
84 observed, typically permafrost degradation has been investigated via long-term monitoring at decadal timescales
85 in response to changes in temperature and precipitation conditions (Åkerman & Johansson, 2008; de la Barreda-
86 Bautista et al., 2022; Olvmo et al., 2020; Sannel et al., 2016). These longer-term studies have shown strong
87 relationships between permafrost degradation and summer temperatures, length of the thaw period, winter
88 precipitation and snow depth (Smith et al., 2022). These types of analyses are very useful for quantifying how
89 much of the landscape has already transitioned and understanding the climate change drivers behind these
90 changes, but they do not capture the initial stages of permafrost degradation in palsas peatlands and the lower
91 rates of subsidence that have yet to result in observable changes in the vegetation or thermokarst formation. The
92 latter is crucial to understand the ongoing response of palsa peatlands to climate warming and to predict when
93 pulses of greenhouse gases to the atmosphere and other impacts (e.g., on infrastructure) are likely to occur.
94 Thus, approaches that detect early signs of degradation at landscape scales, with repeated observations, are
95 urgently required.

96 Due to the vast extent and remoteness of permafrost areas, we looked to satellite remote sensing to underpin the
97 measurement and monitoring assessment of permafrost peatlands, their degradation and resultant climate
98 impacts (Armstrong McKay et al., 2022; Hugelius et al., 2020; Obu, 2021; Schuur et al., 2015; Swingedouw et
99 al., 2020). Optical remote sensing approaches can be augmented with RaDAR remote sensing methods,
100 including InSAR, to capture the early response of permafrost to warming, since these methods can detect
101 vertical land surface motion at millimetre precision across natural landscapes (Alshammari et al., 2020;
102 Alshammari et al., 2018; de la Barreda-Bautista et al., 2022; Short et al., 2014; van Huissteden et al., 2021)
103 (Bartsch *et al.*, 2016). The regular sampling frequency, insensitivity to cloud and, in the case of Sentinel-1, low
104 cost, means InSAR from Sentinel-1 should be well suited to measure and monitor ongoing changes in
105 permafrost affected by climate change. Further, Sentinel-1 for InSAR is effective at both local and regional
106 scales - the 20m × 20m spatial resolution enables measurement of surface motion within local sites (de la
107 Barreda-Bautista et al., 2022), and can do so over entire and complex landscapes, such as the circumpolar
108 permafrost region (Reinosch et al., 2020).

109 The overall aim of this study was to carry out a regional-scale analysis of permafrost degradation across the
110 palsa peatlands of northern Sweden, principally using Sentinel-1 InSAR-derived subsidence as an indication of
111 degradation. Pertinent to this is that any InSAR-detected changes can be associated with known and delineated
112 targets in the wider landscape. Furthermore, it is also important to understand any within-site dynamics of
113 permafrost degradation. This paper therefore has specific objectives to: (i) measure the subsidence rate between
114 2017-2021 of all major palsa peatlands in the northern Sweden region; (ii) determine in which palsa peatlands
115 subsidence is greatest, and (iii) assess if the spatial patterns of degradation can be linked to climatic variables
116 and properties of the different sites across the region. To achieve these objectives, we combined large-scale
117 regional analysis with higher resolution site-specific analysis of patterns in subsidence, using a combination of
118 datasets - satellite (Sentinel-1) InSAR; occupied airborne optical and LiDAR; and snow depth, precipitation, and
119 temperature time-series from meteorological stations across the region.

120

121 2.0 Methodology

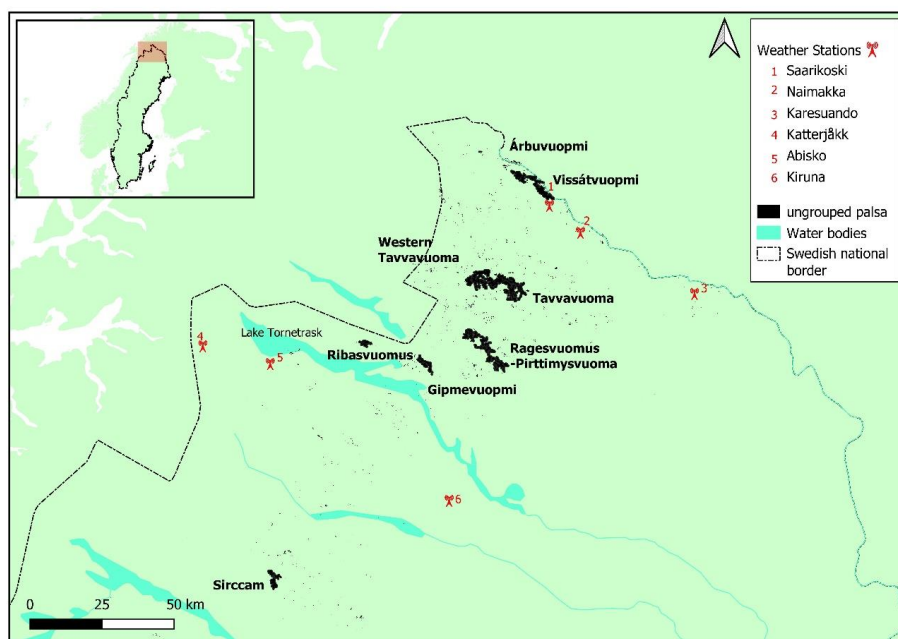
122 2.1 Study area

123 This study focused on the northern part of Sweden; a region containing palsa peatlands, located between 68.84-
124 67.64° N and 18.71-21.19° E. The palsa peatlands of the region are confined predominantly to valley bottoms in
125 an elevation range between ca. 350 and 590m asl (Fig. 1). The rest of the study area region is comprised of
126 forests and/or mountain land covers (Siewert, 2018). Of all the palsas in the region, the eight largest palsa
127 peatlands complexes range between 50 and 273ha in area (Table 1). These were located across the region, which
128 covers a ca. 20,000km² area, with the largest palsa sites located in the north-western parts of the region. Smaller
129 palsa peatlands occur scattered in distribution right across the region. The climate varies across the region from
130 north to south (www.smhi.se). The mean January and July temperatures in Karesuando in the northern part of



131 the study region is -16 and 12.8°C, respectively, while in Kiruna, slightly further south, the mean January and
132 July temperatures is -11.6 and 13.4°C (1991-2020 average). Mean annual precipitation is 443 and 560mm in
133 Karesuando and Kiruna, respectively.

134



135

136 *Figure 1: Map of the palsa peatland complexes in Sweden which were investigated in the study focusing on the*
137 *eight named palsa peatlands. The black regions show where 250m buffers around the palsa areas have created*
138 *continuous expanses (Backe, 2014). Meteorological station positions used in the study are also indicated.*

139

140 We selected larger palsa areas of the region to focus our analysis. This was in line with focus areas by the mapping
141 of palsas undertaken as part of a previous national palsa peatland mapping effort (Backe, 2014). The resultant
142 palsa peatland mapping dataset has a spatial resolution of 100m, with the % palsa cover for each pixel computed,
143 and these pixels given a 250m buffer to produce continuous area outputs. The eight largest continuous areas of
144 these palsa peatlands from the national palsa mapping dataset were selected for this study (Backe, 2014), hereon
145 in referred to as palsa complexes, a term reflecting their mosaic nature of raised palsa plateaux, interspersed with
146 lower lying fen or thermokarst areas. This afforded analyses at a spatial resolution suitable for analysis with
147 Sentinel-1 yet provide practical representation of the condition of the peatland in the region. These eight sites
148 account for the majority of the palsa peatland areas in Sweden, the sites are listed in Table 1 along with some
149 associated information on their status and total and raised palsa plateau areas.

150

151 *Table 1: Information on the major palsa complexes analysed in this paper (Backe, 2014). The protection status*
152 *means no or limited direct anthropogenic activities that may influence palsa degradation. Total site area*
153 *is calculated from the total number of 100m × 100m palsa pixels at each site - these pixels have associated*
154 *percentages for how much of the 100m x 100m area is palsa. The average of these percentages for each site*
155 *displays the palsa density at each site. These percentages are then used to calculate the “total palsa area” for*
156 *each site based on the original report estimates.*



Site Name	Protection Classification	Total site area (ha)	Average extent palsa in these areas (%)	Total palsa area (ha)	Central location (Latitude, Longitude)
Árbuvuopmi	Not protected	327	26.3	86.06	21.03464, 68.83842
Vissátvuopmi	Not protected	867	31.6	273.75	21.19497, 68.79412
Tavvavuoma	EU Nature 2000 SPA, SAC. Site of National Importance for Nature conservation	1719	15.8	271.25	20.85043, 68.51132
Western Tavvavuoma	EU Nature 2000 SPA, SAC. Site of National Importance for Nature conservation	813	13.0	105.74	20.57727, 68.53953
Gipmevuopmi	Pristine mountain forest, Nature reserve, EU Nature 2000 SCI	303	23.0	69.62	20.09767, 68.28377
Ragesvuomus-Pirttimysvuoma	Pristine mountain forest, Nature reserve, EU Nature 2000 SCI	881	6.55	57.74	20.48660, 68.3741
Sirccam	EU Nature 2000 SCI	397	12.8	50.70	18.71528, 67.64537
Ribasvuomus	Pristine mountain forest, Nature reserve, EU Nature 2000 SCI	216	23.2	50.13	19.60100, 68.36116

157

158

159 2.2 Datasets

160 The InSAR-derived dataset of surface motion over this northern Sweden region of study was calculated for the
 161 period between 2017 to 2021, from single look complex C-band SAR data, captured in Interferometric Wide
 162 Swath mode by the Sentinel-1 constellation (European Union’s Copernicus Programme; Torres et al., 2012). SAR
 163 data input were from the thaw season when there was minimal coverage of snow and ice (i.e., between April and
 164 October in each year). Data from descending tracks 168 and 66 were used to cover the target area. Four stacks
 165 were processed independently with one from track 168 and three from track 66, which was split into a northern,
 166 middle, and southern subsets. The APSIS (formerly ISBAS) method (Sowter et al., 2013; Sowter et al., 2016) was
 167 used to characterize surface motion which relaxes the need for consistent phase stability and therefore enables
 168 near-complete spatial and temporal coverage over vegetated surfaces (Alshammari et al., 2020; Alshammari et
 169 al., 2018; Bradley et al., 2022; Cigna & Sowter, 2017; Gee et al., 2017; Sowter et al., 2016), including those found
 170 across snow-free permafrost regions.

171 InSAR processing involved the co-registration of each Sentinel-1 image to a common slant range coordinate
 172 system and multi-looking of data by factors of 7 in range and 2 azimuth. This produced a dataset with an
 173 approximate spatial resolution of 20m × 20m. Using a perpendicular baseline of 250m and maximum temporal
 174 baseline of 183 days ~ 2100 interferograms were generated per stack. The temporal baseline was chosen to
 175 balance the need to reduce the baseline to minimise phase ambiguities and best maintain coherence across the
 176 region, whilst also using a baseline long enough to generate season-to-season pairs over consecutive years. This
 177 is required over permafrost regions to capture more subtle trends of surface motion during the thaw period (de la
 178 Barreda-Bautista et al., 2022; Liu et al., 2010). The interferograms were unwrapped using a modified version of
 179 the SNAPHU algorithm. The multi-annual average velocity was calculated for pixels which maintained a
 180 coherence greater than 0.45 in a minimum of ~ 650 interferograms, with respect to stable reference points located
 181 in the town Kautekenio (N°69.00, E°23.04) for track 168 and Narvik (N°68.44, E°17.42), Kvikkjokk (N°66.95,
 182 E°17.72), and Rognan (N°67.09) for the subsets of track 66. The line-of-sight measurements were converted to
 183 vertical surface displacement using a cosine correction and finally mosaicked into a single deformation product.
 184 Localised UAV studies at sites in Sweden have verified the accuracy of using InSAR to monitor permafrost
 185 degradation (de la Barreda-Bautista et al., 2022).



186 In order to interpret the resultant surface motion dataset produced by the ASPIS InSAR method, two sets of
187 additional data were sourced: (i) higher resolution remote sensing data and (ii) meteorological data. The former
188 included orthophotos captured of the eight target areas by occupied airborne surveys commissioned by the
189 Swedish Survey (www.lantmateriet.se; © Lantmateriet). The orthophotos were panchromatic, with each scene
190 covering a 5km × 5km area, at a 0.5m spatial resolution, the majority were captured in 2016, although gaps were
191 filled with imagery from 2010 and 2008. The Swedish National Digital Elevation Model (DEM), was also used
192 in this study. The DEM was derived via occupied airborne LiDAR data capture in 2016 and processed to compute
193 elevation at 2m spatial resolution across Sweden (www.lantmateriet.se; © Lantmateriet). The orthophotos and
194 DEM provided elevation and landscape characteristics (geomorphic features) for use in this study. The
195 meteorological data was captured by the Swedish Meteorological and Hydrological Institute (www.smhi.se) at
196 meteorological stations across the region. Specifically, the air temperature, precipitation, and snow depth data,
197 were sourced and used from specific stations, i.e., those located closest to the palsa complexes under investigation
198 namely at Katterjåkk, Abisko, Kiruna and Karesuando, Saarikoski/Naimakka (Fig. 1).

199

200 2.3 Data analyses

201 The ASPIS InSAR surface motion dataset was resampled using the mean value from the original 20m × 20m to
202 match the 100m × 100m spatial resolution of the palsa peatland dataset which makes up the eight palsa complexes
203 (Backe 2014). From this the frequency distributions of ASPIS InSAR surface motion at these eight palsa
204 complexes, and over all individual palsa peatland pixels in the region, were produced. Using these data, the
205 maximum and minimum rates of surface motion at each site was determined, as well as the sum of the pixels with
206 palsas that showed subsidence. These derived data relating to surface motion were further interpreted using the
207 orthophotos and DEMs, supported by the meteorological data.

208 The DEM tiles were joined together and clipped to the eight palsa complexes. Following this, the degree of
209 elevation roughness was calculated, via the native topographic roughness index function (Riley, DeGloria, &
210 Elliot, 1999). This roughness index was thresholded at > 0.5 to provide a visual depiction of palsa landform edges
211 in the otherwise typically even terrain of the valley bottoms where the palsas occur. The roughness data was
212 visually compared to the orthophotos from a subset of areas to assess its potential for delineating palsas and this
213 allowed us to determine a threshold value that connected these continuous terrain variables to the specific features
214 of the palsa complexes, such as the raised mound structure of the palsa – so-called palsa mounds (Franklin, 2020).
215 Hillshade was also calculated via the native QGIS function using the default formula, which uses a lighting effect
216 to visualise the roughness of the terrain from differences in local elevation (QGIS, 2022). The roughness,
217 hillshade, and elevation outputs were overlaid on the mapped palsa tiles to provide higher resolution visual
218 interpretation. The roughness and elevation outputs were also resampled to the resolution of the mapped palsa
219 tiles (100m x 100m) to enable statistical comparison. The zonal statistics tool was used to extract mean average
220 values from the resulting roughness and elevation outputs for the 100m spatial resolution mapped palsa tiles.

221 Mean annual, maximum, and minimum daily air temperature, precipitation, and depth of ground snow for the
222 period 2000 to 2022 from the meteorological station nearest to a correspondent palsa complex were extracted and
223 analysed. The Naimakka station did not provide snow depth and the Saarikoski station did not provide air
224 temperature, however, it was deemed that at the regional scale of this study these sites were sufficiently close
225 together (18km) to be interchangeable. Subsequently, data was averaged to provide an annual measurement of each
226 meteorological variable for each station/palsa complex. Due to incomplete meteorological datasets, a longer-term
227 record of the meteorological variables was not possible for all sites. However, long-term climate data (>100years)
228 was available from three meteorological stations in the region: namely, Karesuando, Kiruna, and Abisko. This
229 data was used to assess temporal variability in annual, winter (December, January and February (DJF)) and
230 summer (June, July, and August (JJA)) temperature, precipitation and snowfall since the start of records across
231 the region. Descriptive statistics (mean, minimum, maximum and inter-quartile range) were produced to express
232 the regional differences between these sites. Lastly, to complement the point based meteorological (both weather
233 and climate) data, we used modelled permafrost probabilities based on climatic conditions to explore relationships
234 between climatic conditions and subsidence rates (Obu et al., 2018). In this context, it is worth noting that there
235 may be a mismatch between the modelled permafrost distribution and permafrost in palsa peatlands as this can,
236 in some areas, be a relic of cooler climatic conditions. The mean values from these data on permafrost probability
237 were used to resample to a 100m spatial resolution to enable comparison with the other data sets.



238 To analyse the relationships between surface motion, roughness and percent palsa in each 100m by 100m pixel
239 stratified by palsa complex, SciPy statistics (Virtanen et al., 2020) was used to obtain Pearson's correlation
240 statistics. Pandas (McKinney, 2011) and NumPy (Harris et al., 2020) were used for data management. All scripts
241 are available on the project GitHub (https://github.com/SamValman/Permafrost_Sweden). The relationship
242 between the meteorological variables both over the last two decades at the weather stations closest to the palsa
243 complexes and duration of the climate record at the three weather stations with the longest data series were
244 assessed using regression analysis in Genstat (VNS Ltd). Some of time series were incomplete, in these instances
245 the analysis was conducted using the slightly shorter time series.

246

247 3.0 Results

248 The ASPIS InSAR-derived surface motion outputs for the time-period of interest (2017-2021), ranged between -
249 9.9 and 7.7mm yr⁻¹ across all of the palsa measured, with a mean of 0.05, median of 0.2 and range of 17.7mm yr⁻¹.
250 ¹. Focusing solely on the eight palsa complexes provided greater insight and excluded the most extreme uplift
251 values from scattered individual palsa (Table 2).

252

253 *Table 2: InSAR subsidence and uplift measurements of the palsa complexes defined in Figure 1 and Table 1.*
254 *The total palsa area were used to isolate and extract ASPIS InSAR measurements of surface motion at each of*
255 *the eight sites.*

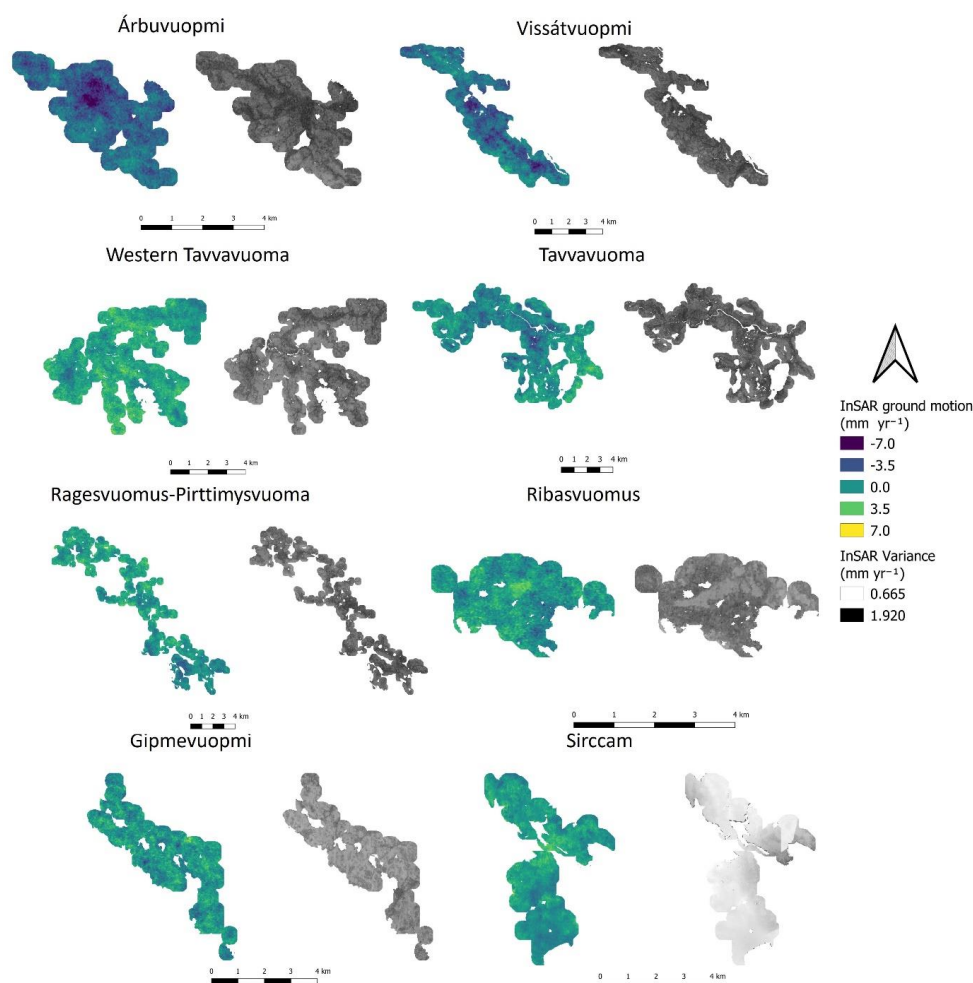
Site	Max subsidence (mm yr ⁻¹)	Max uplift (mm yr ⁻¹)	Subsiding area (ha)	Area subsiding >3.5 mm yr ⁻¹ (ha)
Árbuvuopmi	-9.9	1.7	321.3	138.4
Vissátvuopmi	-8.9	3.5	796.2	204.8
Tavvavuoma	-6.4	6.6	1009.4	50.9
Western				
Tavvavuoma	-5.1	6.3	215.0	1.0
Gipmevuopmi	-6.9	6.3	117.2	1.8
Ragesvuomus-	-5.9	5.7	358.6	7.4
Pirttimysvuoma				
Sirccam	-3.1	5.4	135.3	0.0
Ribasvuomus	-6.5	5.5	93.6	0.7

256

257

258 The spatial plots of surface motion for each palsa complex displayed in Figure 2, illustrates a spatiality in terms
259 of surface motion (both subsidence and uplift and associated variance) across this northern Sweden region. This
260 is evident both within the palsa complexes and between the complexes.

261



262
263

264 *Figure 2: Palsa ground motion measured using Satellite InSAR showing differing levels of degradation across*
265 *the eight study sites. Sites are ordered by their latitudinal position. Negative values correspond to subsidence.*
266 *Note that in order to plot continuous areas the scenes shown are the palsa peatland area plus a 250m buffer*
267 *around each 100m × 100m pixel that cover a minimum of 1% palsa (Backe 2014). This means that areas of non-*
268 *palsa peatland and some areas with mineral soil are included in the figure. ASPIS InSAR variance were less*
269 *than 1.5mm yr⁻¹ in over 90% of pixels.*

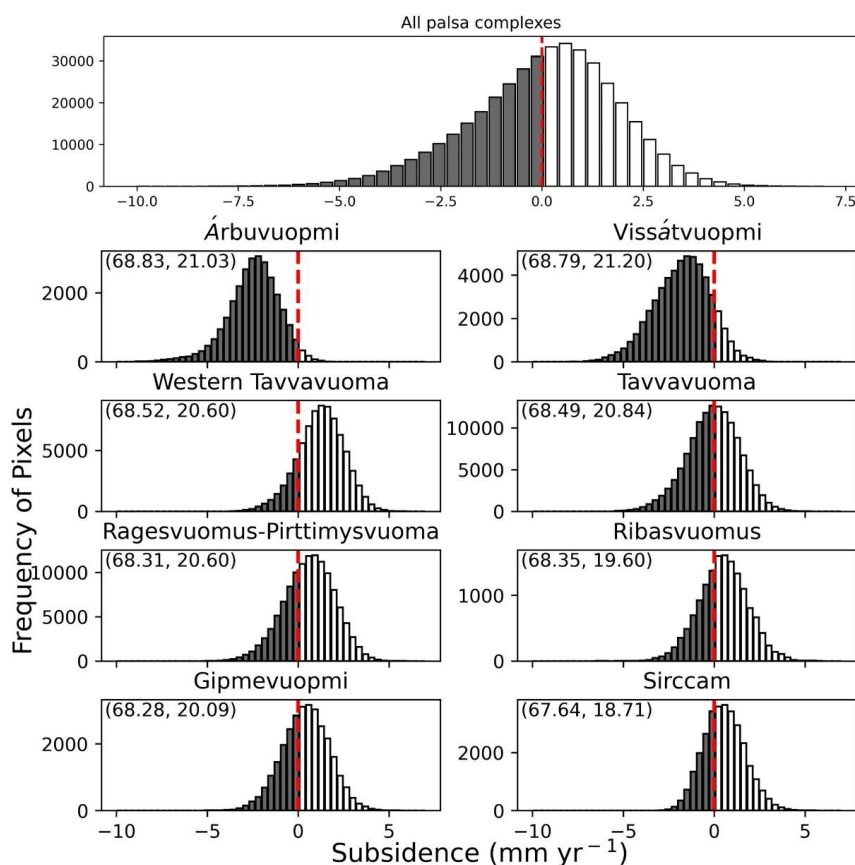
270

271 Subsidence was recorded in just under half of the pixels all the eight palsa complexes (Table 2). Across the target
272 sites 3046.6ha (Table 2) out of the total site area of 5523ha (Table 1) were subsiding, which equates to ca 55% of
273 the total palsa complexes' area. Out of the subsiding parts of the palsa complexes, 405ha were subsiding at rates
274 >3.5mm yr⁻¹ at near gaussian distribution. However, it is evident from the frequency distribution plots, that it is
275 in the palsa complexes in the far north of the region that subsidence dominated the surface motion measured (Table
276 2, Figure 3). At Vissátvuopmi and Árbuvuopmi 98 and 92% of the palsa complexes were subsiding with maximum
277 subsidence rates of -9.9 and -8.9mm yr⁻¹, respectively. The measured area affected by high subsidence rates of
278 between (>3.5mm yr⁻¹) were 204.8ha and 138.4ha at Vissátvuopmi and Árbuvuopmi, respectively. This means
279 that ca. 30% of the total combined area of these two sites (1194ha) is in the highest range of subsidence. The high



280 degree of palsa subsidence at Vissátvuopmi and Árbuvuopmi was confirmed by field observations at these sites
281 (Sofie Sjøgersten, pers. Obs.): Both sites showed signs of active lateral erosions, large scale subsidence and
282 thermokarst formation. The more southerly sites also show subsidence, although rates were much lower, with the
283 -1 and 1 mm yr⁻¹ range being most common (Fig. 3). Areas further to the south and west showed signs of uplift,
284 particularly the western parts of Tavvavuoma and Ribasvuomus with maximum rates of uplift of 6.3 mm across
285 some smaller parts of these sites. However, all sites have some degree of subsidence, albeit at a lower rate
286 compared to the heavily subsiding northern sites.

287



288

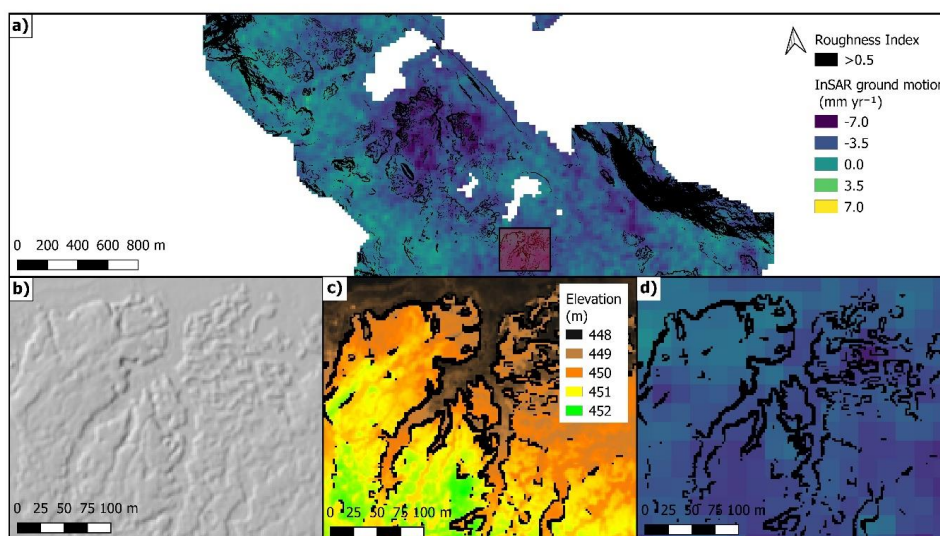
289 *Figure. 3: Distribution of 20m × 20m ASPIS InSAR pixels within each of the palsa complexes in this study and*
290 *the overall trend of the dataset according to the distribution of pixel moving in a particular direction and a given*
291 *rate. Shaded areas with negative values correspond to subsidence. The dashed central lines indicate pixels in*
292 *stable areas with no motion. Central point latitude and longitude is provided for each site in brackets for each*
293 *site.*

294

295 Calculating the roughness index from the DEMs at each palsa complex enabled differentiation of palsa from
296 surrounding lower lying and flat fen areas. Representative example complexes are shown in Figures 4 and 5 -
297 Vissátvuopmi and Western Tavvavuoma. Overall, the palsa complexes to the north (e.g., Fig. 4b, c) display a
298 more pronounced topography across the focus areas than the more south-westerly ones (e.g., Fig. 5b, c). There
299 was clear correspondence between density of palsa and subsidence, i.e., areas with more palsa showed more
300 subsidence (Fig. 4a, d). Furthermore, the palsa complexes showed greater elevation variation compared to



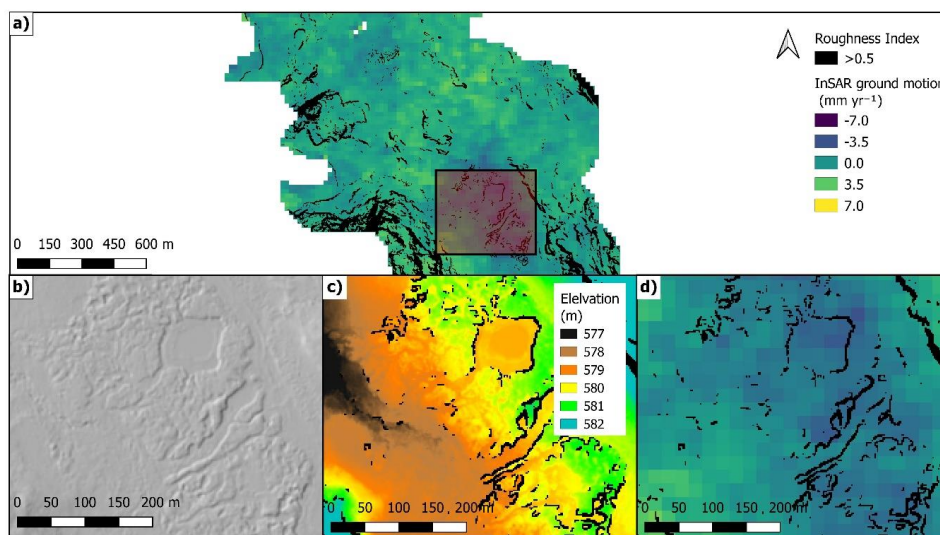
301 surrounding fen areas and were more densely clustered to the north than in the more south westerly sites. These
302 features spatially coincided with higher subsidence. Substantial within site variability in subsidence was evident,
303 where the pixels with the highest subsidence rates being clustered together and following landscapes features,
304 e.g., palsa plateau edges. It was evident that many separate palsa complexes in an area resulted in a high degree
305 of elevation change, causing a high roughness index. In turn, areas with high roughness have the greatest
306 subsidence (Fig. 4,5). Visual comparison between orthophotos and roughness showed that areas of high roughness
307 corresponded well with areas of severe permafrost degradation (as indicated by lateral erosion and thermokarst
308 formation).



309

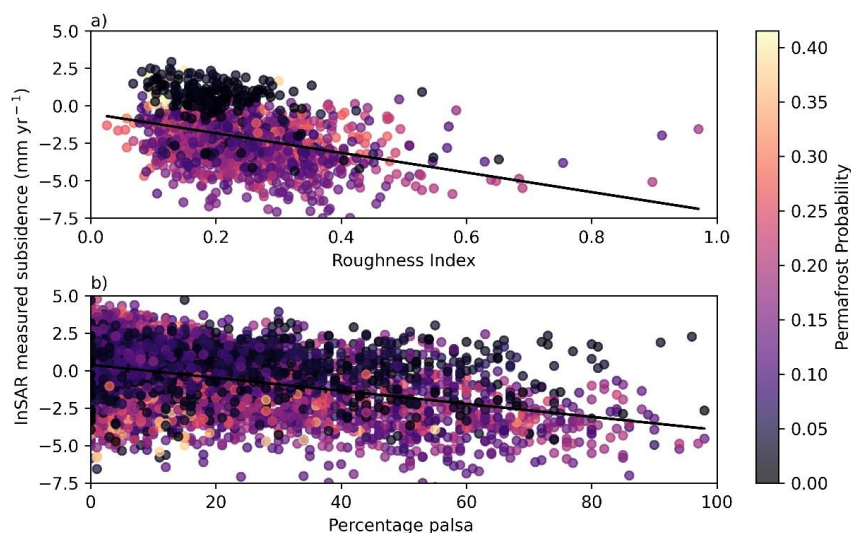
310 *Figure 4: Visual analysis of Vissátvuopmi one of the sites where the most subsidence was found to be*
311 *occurring. Evaluation of correspondence of hillshade DEM (b), DEM (c) and InSAR subsidence (d) with Palsa*
312 *complexes suggested by roughness overlays. The positioning of b,c, and d within the larger site (a) show bands*
313 *of subsidence in proximal to roughness patches suggesting Palsa.*

314



315
316 *Figure 5: Visual analysis of Tavvavuoma which was found to have much lower levels of subsidence in*
317 *comparison to more northern sites. Evaluation of correspondence of hillshade DEM (b), DEM (c) and InSAR*
318 *subsidence (d) with Palsa complexes suggested by roughness overlays. The positioning of b,c, and d within the*
319 *larger site (a) show many less bands of subsidence and potential palsa than Figure 4.*
320

321 Regression analysis showed a relationship between roughness and subsidence as sites with greater subsidence
322 were also found to have greater roughness (Fig. 6a). Higher percentage palsa in a location was linearly related to
323 subsidence with the greatest subsidence found in areas with the highest percentage palsa cover (Fig. 6b). It was
324 also clear that the modelled permafrost probability did not correspond to the percentage of palsa, i.e. pixels with
325 100% palsa are in some instances predicted to have no permafrost (Fig. 6b).

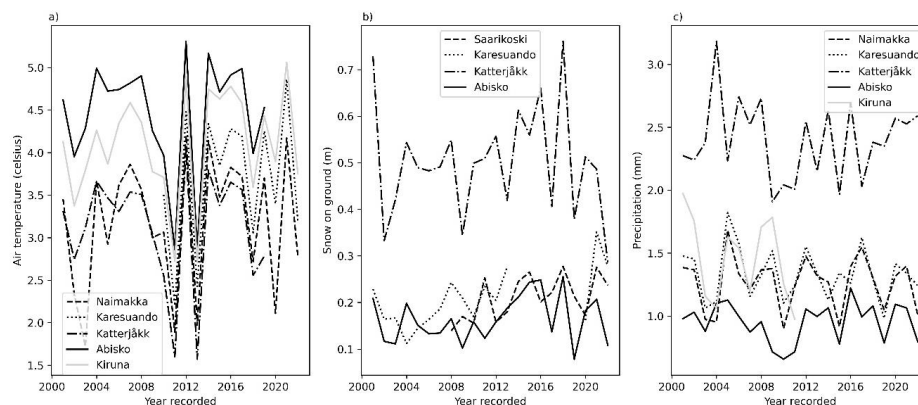


326

327 *Figure 6: Relationship between a) the roughness index; $p < 0.001$, $R^2 = 0.35$ and b) percentage palsa in a*
 328 *pixel; $p < 0.001$, $R^2 = 0.41$ and subsidence. The colours for each data point are the analysed*
 329 *probability (on a scale from 0 to 1) that an area would include permafrost, (Obu et al., 2018). Note that there is*
 330 *less data for the analysis of roughness as the roughness was characterized only for the eight study sites and not*
 331 *all palsa areas. Roughness values from valley sides (which at time were included in the buffer areas) are not*
 332 *used in the figure.*

333

334 The analysis of the metrological data showed variability in both weather and climate across the study region in
 335 part reflecting the patterns in the subsidence data. The warmest minimum and maximum temperatures, -29.2 and
 336 32.8°C respectively, were recorded for the palsa complexes north of Lake Tornetrask, i.e. Gipmevuomi and
 337 Ribasvuomus (Abisko weather station) (Fig. 1). The temperature in the area of Árbuvuopmi, Vissátvuopmi, and
 338 Tavvavuoma palsa complexes (Saarikoski/Naimaka and Karesuando weather stations) ranged between -39.4 and
 339 30.5°C (Table 3, Fig. 7a). The Katterjåkk weather station located in the mountains close to the Norwegian border
 340 recorded the greatest annual snow depth measure of 229cm and a mean of 50cm. Note that in this far western part
 341 of the study area palsa peatland were not present anymore. In contrast, the three other sites had comparable annual
 342 snow depth with a mean of 20-30cm (Table 3, Fig. 7b).



343



344 Figure 7: a) Mean annual daily maximum temperature, b) snow depth on the ground, and c) daily precipitation
 345 at the meteorological stations in the study region (SMHI 2022).

346
 347

348 Table 3: Temperature and snowfall descriptive statistics. The snow depth data are estimated from days with
 349 snow on the ground. Mean annual temperature and precipitation are averaged from 2000 to 2021. Maximum,
 350 minimum and the inter-quartile range of daily maximum temperature and daily precipitation since 2000 are
 351 also shown. Some weather stations lack certain years but were considered to have adequate coverage for this
 352 task while two sites did not have sufficient data collection during the time period to be reliable and were shaded
 353 out.
 354

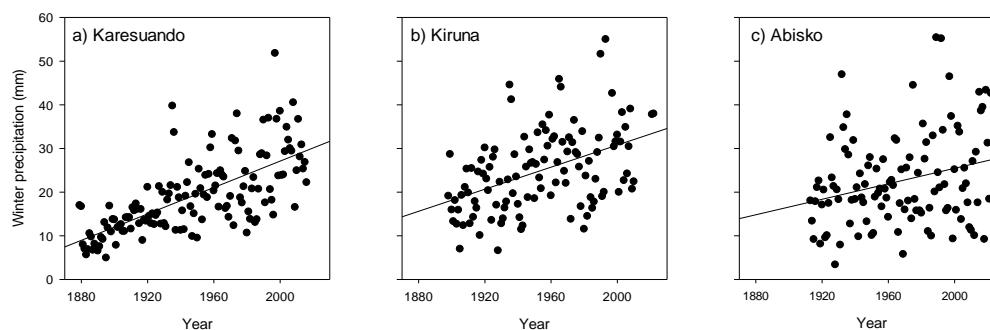
Weather Station	Temperature (°C)				Snow depth (m)			Precipitation (mm)		
	Mean annual	Max daily	Min daily	IQR daily	Mean annual	Max daily	IQR daily	Mean annual	Max daily	IQR daily
Naimakka	-1.40	29.5	-38.2	15.7				456	50.8	1.0
Saarikoski					76.9	0.85	0.43	422	43.6	0.9
Karesuando	-0.70	30.5	-39.4	16.9	75.1	1.00	0.40	490	53.2	1.1
Katterjåkk	-0.32	29.5	-27.6	13	183.0	2.29	0.97	875	104.3	3
Abisko	0.53	32.8	-29.2	13.5	60.0	1.27	0.42	348	61.9	0.6
Kiruna	0.06	30.3	-30.6	15.6	5.3	1.13	0.45	545	53.1	0.9

355

356

357 There was no detectable difference in climatic trends among the meteorological weather stations since 2001 ($p >$
 358 0.05). In contrast, the longer-term climate records show a strong increase in winter precipitation over the last 140
 359 years at Karesuando, the northern most weather station ($F_{1,136}=122.33$, $p < 0.001$; $\square^2=47.0\%$; Fig. 8a). This long-
 360 term trend was also evident, albeit less strong, in Kiruna ($F_{1,110}=28.17$, $p < 0.001$; $\square^2=19.7\%$; Fig. 8b). In Abisko,
 361 the pattern of increasing in winter (DJF) precipitation was less clear ($F_{1,108}=8.29$, $p < 0.01$; $\square^2=6.3\%$; Fig. 8c).
 362 Snow depth, temperature, and summer precipitation (JJA) did not show clear temporal trends (data not shown).

363



364

365 Figure 8. Mean winter (DJF) precipitation over time at a) Karesuando, b) Kiruna, and c) Abisko, significant
 366 trendlines are shown.

367

368 4. Discussion

369 By way of satellite ASPIS InSAR-derived surface motion and associated spatial and statistical analyses, we
 370 have demonstrated on-going, subsidence in the palsa peatlands of northern Sweden driven by a warming
 371 climate. Based on the compelling agreement of subsidence with palsa landforms and their roughness, we
 372 interpret this as permafrost degradation, i.e., thaw of the permafrost core within palsas and disintegration of



373 these landforms. This is in line with a wide range of literature (see introduction) and concurs with the local-scale
374 studies in the area undertaken using both satellite- and field-based methods (de la Barreda-Bautista et al., 2022;
375 Olvmo et al., 2020; Sannel, 2020; Sannel et al., 2016; Sannel & Kuhry, 2011), as well as with, the severe
376 climate warming impacts on temperatures and precipitation noted in the region (Hänsel, 2020; Irannezhad et al.,
377 2017; Vikhamar-Schuler et al., 2016) and the modelled predictions of total loss of permafrost across the region
378 within decades (Fewster et al., 2022). We suggest that the surface subsidence of the sample palsa complexes
379 measured in this study, together with complementary work in Norway (Borge et al., 2017), can be taken as
380 evidence of significant permafrost degradation in all palsa peatland areas across northern Fennoscandia.

381 The processes driving the degradation of the permafrost, as measured by the ASPIS InSAR-derived subsidence
382 data, are complex. Although permafrost degradation was observed in all the palsa complexes, rates varied both
383 within and among palsa complexes (Table 2, Fig. 2 and 3). Overall, the InSAR subsidence data demonstrates a
384 north to south gradient in increasing degradation. This indicates that local factors, such as local climate warming
385 responses or permafrost temperature, determine the sensitivity of particular areas and that regional climatic
386 gradients play a role in the long-term trajectory of these ecosystems (Johansson et al., 2011; Olvmo et al., 2020).
387 In particular, winter precipitation is generally considered a strong predictor of permafrost degradation due to the
388 highly insulating properties of snow, preventing heat dissipation during winter (Olvmo et al., 2020; Seppälä,
389 2011). This points to increased winter precipitation in the part of the northern most part of study areas as a
390 driver of the higher subsidence rates at the northern most palsa complexes (Table 2 and Fig. 7a). Interestingly,
391 climate data from the last two decades did not reveal strong differences in climatic conditions over the area. This
392 suggests that long-term trends combined with a buffered system reaction to change are driving regional patterns
393 in permafrost degradation.

394 It could also be the case that the observed north to south gradient of subsidence rates reflect different phases of
395 progression in an ongoing trend of permafrost degradation across the study region of northern Sweden. It is
396 plausible that the degradation process has progressed further at the more southern sites, reflecting higher
397 permafrost temperatures, and that as a result, subsidence rates have now slowed. All the while at the northern
398 sites, which still have a high cover of palsa: 26.3 and 31.6 % at Årbuvuopmi and Vissátvuopmi respectively,
399 show high subsidence rates. This is supported by research showing rapid permafrost degradation in the
400 southernmost palsa complexes in Sweden (Zuidhoff, 2002; Zuidhoff & Kolstrup, 2000) and in the area around
401 and to the south of Tornetrask, since the 1960's (Åkerman & Johansson, 2008; de la Barreda-Bautista et al.,
402 2022; Varner et al., 2022). However, permafrost degradation in palsa peatlands has progressed over longer-time
403 periods even in the far north of Scandinavia. Here palsas' have decreased in areal extent by 33– 71% over ca. 60
404 years, with more rapid contraction in recent years in Finmarkvidda, Norway and 54% in Vissátvuopmi, northern
405 most Sweden (Borge et al., 2017; Olvmo et al., 2020) and total loss of palsa complexes has been recorded in the
406 far north eastern parts of Norway (Vorren 2017).

407 Although there are differences in subsidence rates among sites the region wide permafrost degradation reflects
408 ongoing climatic trends (Fig. 2 and 6). Since 1901 Scandinavia's climate has become wetter as well as warmer
409 with a greater proportion of the precipitation falling as rain relatively to snow (Hänsel, 2020; Irannezhad et al.,
410 2018; Irannezhad et al., 2017; Vikhamar-Schuler et al., 2016). These trends are reflected in the far north where
411 higher air temperatures, greater precipitation and snow depths has already shifted climatic conditions, in parts of
412 the region, away from those that support permafrost in peatlands e.g. since the 1940's (Åkerman & Johansson,
413 2008; Borge et al., 2017; Olvmo et al., 2020). Further, deep permafrost boreholes show decadal signals of
414 increasing temperatures in the Scandes mountains suggesting that warmer temperatures have been impacting
415 permafrost since the 1920's (Isaksen et al., 2007). Hence, it seems that climate warming has been impacting
416 permafrost in Scandinavia for at least 100 years.

417 As a result of the ongoing trend of increasing permafrost temperatures in palsa peatlands in Scandinavia, their
418 permafrost temperatures are now close to 0°C, making them very vulnerable to decay in response to further
419 increases in temperatures (Christiansen et al., 2010; Farbrot et al., 2013). Palsa formation is closely linked to the
420 mean annual temperature, with temperatures between -1 to -2°C over consecutive years needed as a threshold for
421 palsas to form (Vorren, 2017). In this context it is important to note that the MAT in the area was between 0.53
422 and -1.4°C since 2000 suggesting that at least in parts of the study area the climatic conditions do not support
423 formation of palsa anymore while conditions are marginal for palsa preservation in the entire region.



424 Although subsidence dominated in the northern sites, uplift was also noted in the study region. Mechanisms that
425 may explain patterns of uplift are formation of new palsa as well as short-lived frost mounds that can form
426 temporarily in the palsa system (Zuidhoff, 2002). Further mechanisms that may result in uplift are changes in
427 the water level of the flooded parts of the peatlands as well as accumulation of plant residues from the
428 productive fen vegetation parts of the study sites on the peatland surface, reflecting adaptation of the local
429 ecosystem to degraded palsa mounds reflected by changes in remotely sensed terrain surface.

430 In addition to demonstrating regional permafrost degradation in northern Fennoscandia this work also provides
431 proof of concept for circumpolar assessments of permafrost degradation using ASPIS InSAR. It enables
432 detection of the areas with rapidly degrading permafrost and deepening active layers but also peat consolidation
433 in areas that has already lost its permafrost (de la Barreda-Bautista et al., 2022). The fact that InSAR data is
434 integrated over 20m × 20m pixels means that the signal of local level degradation may be somewhat dampened
435 (de la Barreda-Bautista et al., 2022). However, the high precision of the change in vertical position means that
436 InSAR is an important tool to employ to detect the initial stages of large-scale permafrost degradation.
437 Currently, the study of long-term trends and drivers using InSAR is somewhat limited by the short collection
438 period of Sentinel 1, but as more data are continued to be collected, methods such as non-linear time series
439 creation will become viable to compare subsidence directly to longer climatic drivers. However, the large scale
440 baseline assessment of permafrost subsidence, developed here, provides an initial assessment of ongoing
441 subsidence. would be advantageous should field monitoring be arranged in the future. As a complement to the
442 ASPIS-InSAR data, the novel roughness thresholding method used here together with contextual data proved a
443 powerful tool to map and monitor changes (Franklin, 2020; König et al., 2019; Otto et al., 2012). This approach
444 could be developed using machine learning methods to model palsa dynamics to better automate the extraction
445 of palsa landform positions (König et al., 2019; Luoto & Seppälä, 2002). If accomplished, the operating extent
446 of this tool could be vastly increased using the Arctic 2m DEM dataset over area where its quality is high enough
447 to allow high resolution mapping of the degrading edges of raised palsa plateaus (Morin, 2016). Together the
448 ASPIS-InSAR and the DEM derived roughness index metrics offer novel ways of large scale monitoring of
449 permafrost degradation. This will help to quantify the rate of palsa ecosystem collapse and transition to a non-
450 permafrost state.

451 We conclude that permafrost degradation of palsa peatlands is occurring across northern Sweden, with the
452 greatest rates of degradation and largest areas impacted being Sweden's two largest permafrost peatland
453 complexes in the far north. This raises serious concerns that these systems will lose their permafrost entirely in
454 the coming decades especially as climatic conditions are approaching the limits of sustaining palsa peatlands
455 (Fewster et al., 2022). The implications of this rapid loss of permafrost is ecosystem collapse and loss, as the
456 permafrost core is fundamental to the existence of palsa peatlands. Future research should focus on the
457 implications of this collapse on increased CH₄ emissions (Glagolev et al., 2011; Turetsky et al., 2020; Varner et
458 al., 2022), carbon loss (Hugelius et al., 2020), and thus the potential for strong climate feedbacks (IPCC, 2021)
459 as well as using longer-time InSAR data as this becomes available to investigate regional variations in climatic
460 drivers of permafrost degradation. Further, our study demonstrates that InSAR together with terrain data can be
461 applied over continuous natural surfaces at a regional-scale to monitor permafrost degradation in palsa
462 peatlands, offering a tool for circumpolar monitoring of climate warming impact on these systems.

463

464 5. Acknowledgement

465 This work was supported by funding from the University of Nottingham, UK, EU-InterAct funding via the
466 InterAccess programme and the Swedish research council (VR-2021-05767 to M. Siewert). Associated
467 fieldwork was supported by the Climate Impacts Research Centre (CIRC) at Umeå University. Samuel Valman
468 was supported by the EPSRC funded Geospatial Centre for Doctoral Training (EP/S023577/1).

469

470 6. Author contributions

471 SV: Carried out the majority of the data analysis and made a significant contribution to data interpretation, writ-
472 ing and finalising the manuscript text. Both SV and MS can be considered to have contributed equally to this
473 work.



474 MS: Contributed to the conception of the study, contributed DEM and orthophoto data, carried out fieldwork to
475 assess permafrost degradation, contributed and advised on data analysis and interpretation, contributed to struc-
476 turing, writing, and refining the text. Both MS and SV can be considered to have contributed equally to this
477 work.
478 DB: Contributed to the conception of the study, advised on the data analysis, and made a significant contribution
479 to finalising the text.
480 ML: Provided data analysis, support on the InSAR processing, data interpretation, and writing of the text.
481 DG: Carried out the initial InSAR data processing
482 BBB: Contributed to the conception of the study and refining the text.
483 AS: Contributed to the conception of the study and advised on the InSAR data processing
484 SS: Conceived and directed the study, contributed to data analysis, carried out fieldwork to assess permafrost
485 degradation and made a significant contribution to formulating and finalising the text.
486 SS, DB, AS and MS secured the funding for the project.

487 Code Availability

488
489 All the python scripts used to carry out these analyses are available at the github repository:
490 https://github.com/SamValman/Permafrost_Sweden.

492 Data Availability statement

493
494 The Sentinel-1 datasets are freely available and can be obtained by searching and downloading the Interferomet-
495 ric Wide (IW) swath mode products for orbit track numbers ?? and ?? through the Copernicus Open Access Hub
496 (<https://scihub.copernicus.eu/dhus/#/home>). The processed interferometric data and deformation maps are com-
497 mercially sensitive and may be made available on reasonable request by email addressed to the corresponding
498 author. All other datasets produced during this project will be uploaded on zenodo and the DOI provided once
499 the article has been accepted.

500

501

502

503 References

- 504 Åkerman, H. J., & Johansson, M. (2008). Thawing permafrost and thicker active layers in sub-arctic Sweden.
505 *Permafrost and Periglacial Processes*, 19(3), 279-292. <https://doi.org/10.1002/ppp.626>
- 506 Alshammari, L., Boyd, D. S., Sowter, A., Marshall, C., Andersen, R., Gilbert, P., Marsh, S., & Large, D. J.
507 (2020). Use of Surface Motion Characteristics Determined by InSAR to Assess Peatland Condition
508 [<https://doi.org/10.1029/2018JG004953>]. *Journal of Geophysical Research: Biogeosciences*, 125(1),
509 e2018JG004953. <https://doi.org/https://doi.org/10.1029/2018JG004953>
- 510 Alshammari, L., Large, D. J., Boyd, D. S., Sowter, A., Anderson, R., Andersen, R., & Marsh, S. (2018). Long-
511 Term Peatland Condition Assessment via Surface Motion Monitoring Using the ISBAS DInSAR
512 Technique over the Flow Country, Scotland. *Remote Sensing*, 10(7).
513 <https://doi.org/10.3390/rs10071103>
- 514 Armstrong McKay, D. I., Staal, A., Abrams, J. F., Winkelmann, R., Sakschewski, B., Loriani, S., Fetzner, I.,
515 Cornell, S. E., Rockström, J., & Lenton, T. M. (2022). Exceeding 1.5°C global warming could trigger
516 multiple climate tipping points. *Science*, 377(6611), eabn7950.
517 <https://doi.org/doi:10.1126/science.abn7950>
- 518 Backe, S. (2014). *Kartering av Sveriges palsmyrar*. Länsstyrelsen. Ballantyne C. K. (2018). *Periglacial*
519 *geomorphology*. John Wiley & Sons.
- 520 Bartsch, A., Widhalm, B., Kuhry, P., Hugelius, G., Palmtag, J., Siewert, M.B., 2016. Can C-band synthetic
521 aperture radar be used to estimate soil organic carbon storage in tundra? *Biogeosciences*, 13, 5453-
522 5470.
- 523 Biskaborn, B. K., Smith, S. L., Noetzli, J., Matthes, H., Vieira, G., Streletskiy, D. A., Schoeneich, P.,
524 Romanovsky, V. E., Lewkowicz, A. G., Abramov, A., Allard, M., Boike, J., Cable, W. L.,
525 Christiansen, H. H., Delaloye, R., Diekmann, B., Drozdov, D., Etzelmüller, B., Grosse, G., . . . Lantuit,
526 H. (2019). Permafrost is warming at a global scale. *Nature Communications*, 10(1), 264.
527 <https://doi.org/10.1038/s41467-018-08240-4>
- 528 Borge, A. F., Westermann, S., Solheim, I., & Etzelmüller, B. (2017). Strong degradation of palsas and peat
529 plateaus in northern Norway during the last 60 years. *The Cryosphere*, 11(1), 1-16.
530 <https://doi.org/10.5194/tc-11-1-2017>



- 531 Bradley, A. V., Andersen, R., Marshall, C., Sowter, A., & Large, D. J. (2022). Identification of typical
532 ecohydrological behaviours using InSAR allows landscape-scale mapping of peatland condition. *Earth*
533 *Surf. Dynam.*, 10(2), 261-277. <https://doi.org/10.5194/esurf-10-261-2022>
- 534 Chadburn, S. E., Burke, E. J., Cox, P. M., Friedlingstein, P., Hugelius, G., & Westermann, S. (2017). An
535 observation-based constraint on permafrost loss as a function of global warming. *Nature Climate*
536 *Change*, 7(5), 340-344. <https://doi.org/10.1038/nclimate3262>
- 537 Christiansen, H. H., Eitzelmüller, B., Isaksen, K., Juliussen, H., Farbrøt, H., Humlum, O., Johansson, M.,
538 Ingeman-Nielsen, T., Kristensen, L., Hjort, J., Holmlund, P., Sannel, A. B. K., Sigsgaard, C., Åkerman,
539 H. J., Foged, N., Blikra, L. H., Pernosky, M. A., & Ødegård, R. S. (2010). The thermal state of
540 permafrost in the nordic area during the international polar year 2007–2009. *Permafrost and*
541 *Periglacial Processes*, 21(2), 156-181. <https://doi.org/https://doi.org/10.1002/ppp.687>
- 542 Cigna, F., & Sowter, A. (2017). The relationship between intermittent coherence and precision of ISBAS InSAR
543 ground motion velocities: ERS-1/2 case studies in the UK. *Remote Sensing of Environment*, 202, 177-
544 198. <https://doi.org/https://doi.org/10.1016/j.rse.2017.05.016>
- 545 de la Barrada-Bautista, B., Boyd, D. S., Ledger, M., Siewert, M. B., Chandler, C., Bradley, A. V., Gee, D.,
546 Large, D. J., Olofsson, J., Sowter, A., & Sjögersten, S. (2022). Towards a Monitoring Approach for
547 Understanding Permafrost Degradation and Linked Subsidence in Arctic Peatlands. *Remote Sensing*,
548 14(3). <https://doi.org/10.3390/rs14030444>
- 549 Douglas, T. A., Hiemstra, C. A., Anderson, J. E., Barbato, R. A., Bjella, K. L., Deeb, E. J., Gelvin, A. B.,
550 Nelsen, P. E., Newman, S. D., Saari, S. P., & Wagner, A. M. (2021). Recent degradation of interior
551 Alaska permafrost mapped with ground surveys, geophysics, deep drilling, and repeat airborne lidar.
552 *The Cryosphere*, 15(8), 3555-3575. <https://doi.org/10.5194/tc-15-3555-2021>
- 553 Douglas, T. A., Jorgenson, M. T., Brown, D. R. N., Campbell, S. W., Hiemstra, C. A., Saari, S. P., Bjella, K., &
554 Liljedahl, A. K. (2015). Degrading permafrost mapped with electrical resistivity tomography, airborne
555 imagery and LiDAR, and seasonal thaw measurements. *GEOPHYSICS*, 81(1), WA71-WA85.
556 <https://doi.org/10.1190/geo2015-0149.1>
- 557 Farbrøt, H., Isaksen, K., Eitzelmüller, B., & Gislås, K. (2013). Ground Thermal Regime and Permafrost
558 Distribution under a Changing Climate in Northern Norway. *Permafrost and Periglacial Processes*,
559 24(1), 20-38. <https://doi.org/https://doi.org/10.1002/ppp.1763>
- 560 Fewster, R. E., Morris, P. J., Ivanovic, R. F., Swindles, G. T., Peregon, A. M., & Smith, C. J. (2022). Imminent
561 loss of climate space for permafrost peatlands in Europe and Western Siberia. *Nature Climate Change*,
562 12(4), 373-379. <https://doi.org/10.1038/s41558-022-01296-7>
- 563 Franklin, S. E. (2020). Interpretation and use of geomorphometry in remote sensing: a guide and review of
564 integrated applications. *International Journal of Remote Sensing*, 41(19), 7700-7733.
565 <https://doi.org/10.1080/01431161.2020.1792577>
- 566 Fronzek, S., Luoto, M., & Carter, T. (2006). Potential effect of climate change on the distribution of palsa mires
567 in subarctic Fennoscandia. *Climate Research*, 32(1), 1-12. [https://www.int-](https://www.int-res.com/abstracts/cr/v32/n1/p1-12/)
568 [res.com/abstracts/cr/v32/n1/p1-12/](https://www.int-res.com/abstracts/cr/v32/n1/p1-12/)
- 569 Gee, D., Bateson, L., Sowter, A., Grebby, S., Novellino, A., Cigna, F., Marsh, S., Banton, C., & Wyatt, L.
570 (2017). Ground Motion in Areas of Abandoned Mining: Application of the Intermittent SBAS (ISBAS)
571 to the Northumberland and Durham Coalfield, UK. *Geosciences*, 7(3).
572 <https://doi.org/10.3390/geosciences7030085>
- 573 Gislås, K., Eitzelmüller, B., Lussana, C., Hjort, J., Sannel, A. B. K., Isaksen, K., Westermann, S., Kuhry, P.,
574 Christiansen, H. H., Frampton, A., & Åkerman, J. (2017). Permafrost Map for Norway, Sweden and
575 Finland. *Permafrost and Periglacial Processes*, 28(2), 359-378.
576 <https://doi.org/https://doi.org/10.1002/ppp.1922>
- 577 Glagolev, M., Kleptsova, I., Filippov, I., Maksyutov, S., & Machida, T. (2011). Regional methane emission
578 from West Siberia mire landscapes. *Environmental Research Letters*, 6(4), 045214.
- 579 Hänsel, S. (2020). Changes in the Characteristics of Dry and Wet Periods in Europe (1851–2015). *Atmosphere*,
580 11(10), 1080. <https://www.mdpi.com/2073-4433/11/10/1080>
- 581 Harris, C. R., Millman, K. J., van der Walt, S. J., Gommers, R., Virtanen, P., Cournapeau, D., Wieser, E.,
582 Taylor, J., Berg, S., Smith, N. J., Kern, R., Picus, M., Hoyer, S., van Kerkwijk, M. H., Brett, M.,
583 Haldane, A., del Río, J. F., Wiebe, M., Peterson, P., . . . Oliphant, T. E. (2020). Array programming
584 with NumPy. *Nature*, 585(7825), 357-362. <https://doi.org/10.1038/s41586-020-2649-2>
- 585 Harris, L. I., Richardson, K., Bona, K. A., Davidson, S. J., Finkelstein, S. A., Garneau, M., McLaughlin, J.,
586 Nwaishi, F., Olefeldt, D., Packalen, M., Roulet, N. T., Southee, F. M., Strack, M., Webster, K. L.,
587 Wilkinson, S. L., & Ray, J. C. (2022). The essential carbon service provided by northern peatlands.
588 *Frontiers in Ecology and the Environment*, 20(4), 222-230.
589 <https://doi.org/https://doi.org/10.1002/fee.2437>



- 590 Hugelius, G. A., Loisel, J. A., Chadburn, S. A., Jackson, R. A., Jones, M. A., MacDonald, G., Maruschak, M.,
591 Olefeldt, D. A., Packalen, M., Siewert, M. A., Treat, C. A.-O., Turetsky, M., Voigt, C. A., & Yu, Z. A.
592 (2020). Large stocks of peatland carbon and nitrogen are vulnerable to permafrost thaw. *Proceedings of*
593 *the National Academy of Sciences*, 117(34), 20438-20446. <https://doi.org/10.1073/pnas.1916387117>.
- 594 IPCC. (2021). *The Physical Science Basis. Contribution of Working Group I to the Sixth Assessment Report of*
595 *the Intergovernmental Panel on Climate Change*. Cambridge University Press.
- 596 Irannezhad, M., Moradkhani, H., & Kløve, B. (2018). Spatiotemporal Variability and Trends in Extreme
597 Temperature Events in Finland over the Recent Decades: Influence of Northern Hemisphere
598 Teleconnection Patterns. *Advances in Meteorology*, 2018, 7169840.
599 <https://doi.org/10.1155/2018/7169840>
- 600 Irannezhad, M., Ronkanen, A.-K., Kiani, S., Chen, D., & Kløve, B. (2017). Long-term variability and trends in
601 annual snowfall/total precipitation ratio in Finland and the role of atmospheric circulation patterns.
602 *Cold Regions Science and Technology*, 143, 23-31.
603 <https://doi.org/https://doi.org/10.1016/j.coldregions.2017.08.008>
- 604 Isaksen, K., Sollid, J. L., Holmlund, P., & Harris, C. (2007). Recent warming of mountain permafrost in
605 Svalbard and Scandinavia. *Journal of Geophysical Research: Earth Surface*, 112(F2).
606 <https://doi.org/https://doi.org/10.1029/2006JF000522>
- 607 Johansson, M., Åkerman, J., Keuper, F., Christensen, T. R., Lantuit, H., & Callaghan, T. V. (2011). Past and
608 Present Permafrost Temperatures in the Abisko Area: Redrilling of Boreholes. *AMBIO*, 40(6), 558.
609 <https://doi.org/10.1007/s13280-011-0163-3>
- 610 Johansson, M., Callaghan, T. V., Bosiö, J., Åkerman, H. J., Jackowicz-Korczynski, M., & Christensen, T. R.
611 (2013). Rapid responses of permafrost and vegetation to experimentally increased snow cover in sub-
612 arctic Sweden. *Environmental Research Letters*, 8(3), 035025. [https://doi.org/10.1088/1748-](https://doi.org/10.1088/1748-9326/8/3/035025)
613 [9326/8/3/035025](https://doi.org/10.1088/1748-9326/8/3/035025)
- 614 Köchy, M., Hiederer, R., & Freibauer, A. (2015). Global distribution of soil organic carbon – Part 1: Masses and
615 frequency distributions of SOC stocks for the tropics, permafrost regions, wetlands, and the world.
616 *SOIL*, 1(1), 351-365. <https://doi.org/10.5194/soil-1-351-2015>
- 617 König, S., Schultz, J. A., Schoch, A., Blöthe, J., Schrott, L., & Thonfeld, F. (2019). Mountain Permafrost
618 Distribution Modeling—A Geomorphometry-Remote Sensing Approach for the Hohe Tauern National
619 Park, Austria. *Dreiländertagung der DGPF, der OVG und der SGPF in Wien, Österreich—*
620 *Publikationen der DGPF*, 28.
- 621 Könönen, O. H., Karjalainen, O., Aalto, J., Luoto, M., & Hjort, J. (2022). Environmental spaces for palsas and
622 peat plateaus are disappearing at a circumpolar scale. *The Cryosphere Discuss.*, 2022, 1-37.
623 <https://doi.org/10.5194/tc-2022-135>
- 624 Liu, L., Zhang, T., & Wahr, J. (2010). InSAR measurements of surface deformation over permafrost on the
625 North Slope of Alaska. *Journal of Geophysical Research: Earth Surface*, 115(F3).
626 <https://doi.org/10.1029/2009JF001547>
- 627 Luoto, M., & Seppälä, M. (2002). Modelling the distribution of palsas in Finnish Lapland with logistic
628 regression and GIS. *Permafrost and Periglacial Processes*, 13(1), 17-28.
- 629 Luoto, M., & Seppälä, M. (2003). Thermokarst ponds as indicators of the former distribution of palsas in
630 Finnish Lapland. *Permafrost and Periglacial Processes*, 14(1), 19-27. <https://doi.org/10.1002/ppp.441>
- 631 Mamet, S. D., Chun, K. P., Kershaw, G. G. L., Loranty, M. M., & Kershaw, G. P. (2017). Recent Increases in
632 Permafrost Thaw Rates and Areal Loss of Palsas in the Western Northwest Territories, Canada.
633 *Permafrost and Periglacial Processes*, 28, 619-633. <https://doi.org/10.1002/ppp.1951>
- 634 Markkula, I., Turunen, M., & Rasmus, S. (2019). A review of climate change impacts on the ecosystem services
635 in the Saami Homeland in Finland. *Science of The Total Environment*, 692, 1070-1085.
636 <https://doi.org/https://doi.org/10.1016/j.scitotenv.2019.07.272>
- 637 Matthews, J. A., Dahl, S.-O., Berrisford, M. S., & Nesje, A. (1997). Cyclic Development and Thermokarstic
638 Degradation of Palsas in the Mid-Alpine Zone at Leirpullan, Dovrefjell, Southern Norway. *Permafrost*
639 *and Periglacial Processes*, 8(1), 107-122. [https://doi.org/https://doi.org/10.1002/\(SICI\)1099-](https://doi.org/https://doi.org/10.1002/(SICI)1099-1530(199701)8:1<107::AID-PPP237>3.0.CO;2-Z)
640 [1530\(199701\)8:1<107::AID-PPP237>3.0.CO;2-Z](https://doi.org/https://doi.org/10.1002/(SICI)1099-1530(199701)8:1<107::AID-PPP237>3.0.CO;2-Z)
- 641 McKinney, W. (2011). pandas: a Foundational Python Library for Data Analysis and Statistics.
- 642 Miglovet, M., Zagirova, S., Goncharova, N., & Mikhailov, O. (2021). Methane Emission from Palsa Mires in
643 Northeastern European Russia. *Russian Meteorology and Hydrology*, 46(1), 52-59.
644 <https://doi.org/10.3103/S1068373921010076>
- 645 Morin, P., Porter, C., Cloutier, M., Howat, I., Noh, M.J., Willis, M., Bates, B., Williamson, C. and Peterman, K.
646 (2016). ArcticDEM; a publicly available, high resolution elevation model of the Arctic. EGU General
647 Assembly 2016, Vienna, Austria.
- 648 Obu, J. (2021). How Much of the Earth's Surface is Underlain by Permafrost? *Journal of Geophysical Research:*
649 *Earth Surface*, 126(5), e2021JF006123. <https://doi.org/https://doi.org/10.1029/2021JF006123>



- 650 Obu, J., Westermann, S., Kääb, A., & Bartsch, A. (2018). *Ground Temperature Map, 2000-2016, Northern*
651 *Hemisphere Permafrost PANGAEA*. <https://doi.org/10.1594/PANGAEA.888600>
- 652 Olvmo, M., Holmer, B., Thorsson, S., Reese, H., & Lindberg, F. (2020). Sub-arctic palsa degradation and the
653 role of climatic drivers in the largest coherent palsa mire complex in Sweden (Vissátvuopmi), 1955–
654 2016. *Scientific Reports*, 10(1), 8937. <https://doi.org/10.1038/s41598-020-65719-1>
- 655 Otto, J. c., Keuschnig, M., Götz, J., Marbach, M., & Schrott, L. (2012). Detection of mountain permafrost by
656 combining high resolution surface and subsurface information—an example from the Glatzbach
657 catchment, Austrian Alps. *Geografiska Annaler: Series A, Physical Geography*, 94(1), 43-57.
658 <https://doi.org/10.1111/j.1468-0459.2012.00455.x>
- 659 QGIS, D. (2022). QGIS User Guide: 24.2.1 Raster Analysis. Retrieved from
660 https://docs.qgis.org/3.16/en/docs/user_manual/processing_algs/gdal/rasteranalysis.html#hillshade
- 661 Ramage, J., Jungsberg, L., Wang, S. N., Westermann, S., Lantuit, H., & Heleniak, T. (2021). Population living
662 on permafrost in the Arctic. *Population and Environment*, 43(1), 22-38.
663 <https://doi.org/10.1007/s11111-020-00370-6>
- 664 Reinosch, E., Buckel, J., Dong, J., Gerke, M., Baade, J., & Riedel, B. (2020). InSAR time series analysis of
665 seasonal surface displacement dynamics on the Tibetan Plateau. *The Cryosphere*, 14(5), 1633-1650.
666 <https://doi.org/10.5194/tc-14-1633-2020>
- 667 Sannel, A. B. K. (2020). Ground temperature and snow depth variability within a subarctic peat plateau
668 landscape. *Permafrost and Periglacial Processes*, 31(2), 255-263. <https://doi.org/10.1002/ppp.2045>
- 669 Sannel, A. B. K., Hugelius, G., Jansson, P., & Kuhry, P. (2016). Permafrost Warming in a Subarctic Peatland –
670 Which Meteorological Controls are Most Important?. *Permafrost and Periglacial Processes*, 27(2),
671 177-188. <https://doi.org/10.1002/ppp.1862>
- 672 Sannel, A. B. K., & Kuhry, P. (2011). Warming-induced destabilization of peat plateau/thermokarst lake
673 complexes. *Journal of Geophysical Research: Biogeosciences*, 116(G3).
674 <https://doi.org/10.1029/2010JG001635>
- 675 Schuur, E. A. G., McGuire, A. D., Schädel, C., Grosse, G., Harden, J. W., Hayes, D. J., Hugelius, G., Koven, C.
676 D., Kuhry, P., Lawrence, D. M., Natali, S. M., Olefeldt, D., Romanovsky, V. E., Schaefer, K.,
677 Turetsky, M. R., Treat, C. C., & Vonk, J. E. (2015). Climate change and the permafrost carbon
678 feedback. *Nature*, 520(7546), 171-179. <https://doi.org/10.1038/nature14338>
- 679 Schuur, E. A. G., Vogel, J. G., Crummer, K. G., Lee, H., Sickman, J. O., & Osterkamp, T. E. (2009). The effect
680 of permafrost thaw on old carbon release and net carbon exchange from tundra. *Nature*, 459(7246),
681 556-559. <https://doi.org/10.1038/nature08031>
- 682 Seppälä, M. (2011). Synthesis of studies of palsa formation underlining the importance of local environmental
683 and physical characteristics. *Quaternary Research*, 75(2), 366-370.
684 <https://doi.org/10.1016/j.yqres.2010.09.007>
- 685 Siewert, M.B., 2018. High-resolution digital mapping of soil organic carbon in permafrost terrain using machine
686 learning: a case study in a sub-Arctic peatland environment. *Biogeosciences*, 15, 1663-1682.
- 687 Sjöberg, Y., Siewert, M.B., Rudy, A.C.A., Paquette, M., Bouchard, F., Malenfant-Lepage, J., Fritz, M., 2020.
688 Hot trends and impact in permafrost science. *Permafrost and Periglacial Processes*, 31, 461-471.
- 689 Short, N., LeBlanc, A.-M., Sladen, W., Oldenborger, G., Mathon-Dufour, V., & Brisco, B. (2014).
690 RADARSAT-2 D-InSAR for ground displacement in permafrost terrain, validation from Iqaluit
691 Airport, Baffin Island, Canada. *Remote Sensing of Environment*, 141, 40-51.
692 <https://doi.org/https://doi.org/10.1016/j.rse.2013.10.016>
- 693 SMHI, (2022). Download Meteorological observations. Retrieved from
694 [https://www.smhi.se/data/meteorologi/ladda-ner-meteorologiska-
695 observationer#param=airtemperature&instant_stations=core.stationid=191910](https://www.smhi.se/data/meteorologi/ladda-ner-meteorologiska-observationer#param=airtemperature&instant_stations=core.stationid=191910)
- 696 Smith, M. W., & Riseborough, D. W. (1996). Permafrost monitoring and detection of climate change.
697 *Permafrost and Periglacial Processes*, 7(4), 301-309.
698 [https://doi.org/https://doi.org/10.1002/\(SICI\)1099-1530\(199610\)7:4<301::AID-PPP231>3.0.CO;2-R](https://doi.org/https://doi.org/10.1002/(SICI)1099-1530(199610)7:4<301::AID-PPP231>3.0.CO;2-R)
- 699 Smith, S.L, O'Neill, H.B., Isaksen, K., Noetzli, J. and Romanovsky, V.E. (2022). The changing thermal state of
700 permafrost. *Nature Reviews Earth and Environment*, 3, 10-23.
- 701 Sowter, A., Bin Che Amat, M., Cigna, F., Marsh, S., Athab, A., & Alshammari, L. (2016). Mexico City land
702 subsidence in 2014–2015 with Sentinel-1 IW TOPS: Results using the Intermittent SBAS (ISBAS)
703 technique. *International Journal of Applied Earth Observation and Geoinformation*, 52, 230-242.
704 <https://doi.org/https://doi.org/10.1016/j.jag.2016.06.015>
- 705 Spyder Website Contributors. (2021). Spyder IDE. Retrieved from <https://www.spyder-ide.org/>
- 706 Swingedouw, D., Ifejika Speranza, C., Bartsch, A., Durand, G., Jamet, C., Beaugrand, G., & Conversi, A.
707 (2020). Early Warning from Space for a Few Key Tipping Points in Physical, Biological, and Social-
708 Ecological Systems. *Surveys in Geophysics*, 41(6), 1237-1284. [https://doi.org/10.1007/s10712-020-
709 09604-6](https://doi.org/10.1007/s10712-020-09604-6)



- 710 Tarnocai, C., Canadell, J. G., Schuur, E. A. G., Kuhry, P., Mazhitova, G., & Zimov, S. (2009). Soil organic
711 carbon pools in the northern circumpolar permafrost region. *Global Biogeochemical Cycles*, 23(2).
712 <https://doi.org/https://doi.org/10.1029/2008GB003327>
- 713 Torres, R., Snoeij, P., Geudtner, D., Bibby, D., Davidson, M., Attema, E., Potin, P., Rommen, B., Flourey, N.,
714 Brown, M., Traver, I. N., Deghaye, P., Duesmann, B., Rosich, B., Miranda, N., Bruno, C., L'Abbate,
715 M., Croci, R., Pietropaolo, A., . . . Rostan, F. (2012). GMES Sentinel-1 mission. *Remote Sensing of*
716 *Environment*, 120, 9-24. <https://doi.org/https://doi.org/10.1016/j.rse.2011.05.028>
- 717 Turetsky, M. R., Abbott, B. W., Jones, M. C., Anthony, K. W., Olefeldt, D., Schuur, E. A. G., Grosse, G.,
718 Kuhry, P., Hugelius, G., Koven, C., Lawrence, D. M., Gibson, C., Sannel, A. B. K., & McGuire, A. D.
719 (2020). Carbon release through abrupt permafrost thaw. *Nature Geoscience*, 13(2), 138-143.
720 <https://doi.org/10.1038/s41561-019-0526-0>
- 721 Vallée, S., & Payette, S. (2007). Collapse of permafrost mounds along a subarctic river over the last 100 years
722 (northern Québec). *Geomorphology*, 90, 162-170. <https://doi.org/10.1016/j.geomorph.2007.01.019>
- 723 van Huissteden, J., Teshebaeva, K., Cheung, Y., Magnússon, R. Í., Noorbergen, H., Karsanaev, S. V., Maximov,
724 T. C., & Dolman, A. J. (2021). Geomorphology and InSAR-Tracked Surface Displacements in an Ice-
725 Rich Yedoma Landscape. *Frontiers in Earth Science*, 9(724).
726 <https://doi.org/10.3389/feart.2021.680565>
- 727 Varner, R. K., Crill, P. M., Frohling, S., McCalley, C. K., Burke, S. A., Chanton, J. P., Holmes, M. E., null, n.,
728 Saleska, S., & Palace, M. W. (2022). Permafrost thaw driven changes in hydrology and vegetation
729 cover increase trace gas emissions and climate forcing in Stordalen Mire from 1970 to 2014.
730 *Philosophical Transactions of the Royal Society A: Mathematical, Physical and Engineering Sciences*,
731 380(2215), 20210022. <https://doi.org/10.1098/rsta.2021.0022>
- 732 Vikhamar-Schuler, D., Isaksen, K., Haugen, J. E., Tømmervik, H., Luks, B., Schuler, T. V., & Bjerke, J. W.
733 (2016). Changes in Winter Warming Events in the Nordic Arctic Region. *Journal of Climate*, 29(17),
734 6223-6244. <https://doi.org/10.1175/JCLI-D-15-0763.1>
- 735 Virtanen, P., Gommers, R., Oliphant, T. E., Haberland, M., Reddy, T., Cournapeau, D., Burovski, E., Peterson,
736 P., Weckesser, W., & Bright, J. (2020). SciPy 1.0: fundamental algorithms for scientific computing in
737 Python. *Nature methods*, 17(3), 261-272.
- 738 Vorren, K.-D. (2017). The first permafrost cycle in Færdesmyra, eastern Finnmark, Norway? *Norsk Geografisk*
739 *Tidsskrift - Norwegian Journal of Geography*, 71(2), 114-121.
740 <https://doi.org/10.1080/00291951.2017.1316309>
- 741 Zuidhoff, F. S. (2002). Recent decay of a single palsa in relation to weather conditions between 1996 and 2000
742 in Laivadalen, northern Sweden. *Geografiska Annaler Series A-Physical Geography*, 84A(2), 103-111.
743 <https://doi.org/10.1111/j.0435-3676.2002.00164.x>
- 744 Zuidhoff, F. S., & Kolstrup, E. (2000). Changes in palsa distribution in relation to climate change in Laivadalen,
745 northern Sweden, especially 1960–1997. *Permafrost and Periglacial Processes*, 11(1), 55-69.
746 [https://doi.org/https://doi.org/10.1002/\(SICI\)1099-1530\(200001/03\)11:1](https://doi.org/https://doi.org/10.1002/(SICI)1099-1530(200001/03)11:1)